ACS APPLIED MATERIALS & INTERFACES

Research Article

www.acsami.org

Hard X-ray Photoelectron Spectroscopy (HAXPES) Investigation of the Silicon Solid Electrolyte Interphase (SEI) in Lithium-Ion Batteries

Benjamin T. Young,[†,‡] David R. Heskett,[†] Cao Cuong Nguyen,[§] Mengyun Nie,[§] Joseph C. Woicik,[∥] and Brett L. Lucht*[,§]

[†]Department of Physics and [§]Department of Chemistry, University of Rhode Island, Kingston Rhode Island 02881, United States

[‡]Physical Sciences Department, Rhode Island College, Providence Rhode Island 02908, United States

[∥]National Institute of Standards and Technology, Gaithersburg, Maryland 20899, United States

ABSTRACT: Binder-free silicon (BF-Si) nanoparticle anodes were cycled with 1.2 M $LiPF_6$ in ethylene carbonate (EC), fluoroethylene carbonate (FEC), or EC with 15% FEC (EC:FEC), extracted from cells and analyzed by Hard X-ray Photoelectron Spectroscopy (HAXPES). All of the electrolytes generate an SEI which is integrated with Si containing species. The EC and EC:FEC electrolytes result in the generation of Li_xSiO_y after the first cycle while Li_xSiO_y is only observed after five cycles for the FEC electrolyte. The SEI initially generated from the EC electrolyte is primarily composed of lithium ethylene dicarbonate (LEDC) and LiF. However, after five cycles, the composition changes, especially near the surface of silicon because of decomposition of the LEDC. The SEI generated from the EC:FEC electrolytes contains LEDC, LiF, and poly(FEC) and small changes are observed upon additional cycling. The SEI generated with the FEC electrolyte contains LiF and poly(FEC) and small changes are observed upon additional cycling. The stability of the SEI correlates with the observed capacity retention of the cells.

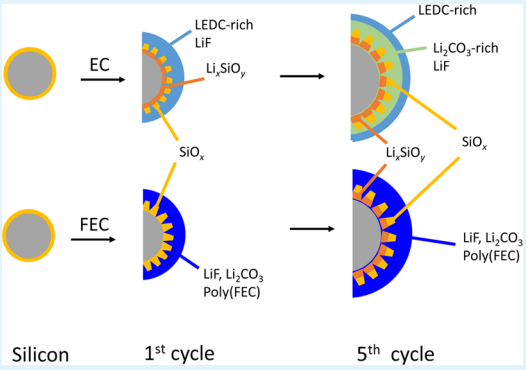

KEYWORDS: *HAXPES, XPS, solid electrolyte interface, Silicon anode, electrolyte additives, lithium ion battery, ex-situ surface analysis*

INTRODUCTION

The demand for increased energy density in lithium-ion batteries necessitates a move away from the industry standard graphite anode. With a theoretical specific capacity of 3580 mAh/g, silicon can offer an increase of almost an order of magnitude over graphite (372 mAh/g).[1] However, in conjunction with the increased capacity, the silicon anode experiences a ~ 280% change in volume upon lithiation. During charge/discharge cycling, silicon volume fluctuations subject the electrode to large mechanical stresses. Associated effects include fracturing of the silicon particles, damaging the electrical contact of the electrode material with the current collector, and repeated destruction and formation of the solid electrolyte interphase (SEI).[2−4]

Two of the main methods to improve the performance of silicon anodes include novel anode structures and variation of the electrolyte composition. The design of nanostructured silicon materials has improved the performance of silicon anodes by limiting the mechanical damage to the electrode particles.[4−8] Alternatively, the development of novel electrolytes can improve the performance of silicon anodes via the generation of a superior anode SEI. The SEI must have good lithium-ion conduction, but be electrically insulating to prevent further reduction of the electrolyte by the lithiated silicon surface. The SEI must also remain stable under the expansion and contraction of the silicon particles. The structure of the silicon anode SEI has typically been modified by the incorporation of sacrificial electrolyte additives that react with the surface of the silicon to generate an SEI with greater mechanical stability.[5,9−16]

There have been several investigations of the SEI generated on silicon nanoparticle anodes.[12,15−18] Most of these investigations support a similar composition to the SEI observed on graphite anodes. However, the SEI on silicon anodes has been reported to be more integrated with the active material than is typically observed for graphite.[17] The SEI generated on silicon nanoparticles cycled with $LiPF_6$ in ethylene carbonate (EC)/diethyl carbonate (DEC) electrolyte is dominated by lithium alkyl carbonates in the outer SEI while the inner SEI is intermixed with Li_xSiO_y from the conversion of the surface oxide layer of the silicon.[17] However, these investigations were complicated by the presence of CMC binder and carbon black because these components can overlap with the spectral features of the SEI. Inclusion of fluoroethylene carbonate (FEC) in the electrolyte has been investigated with significant improvement in capacity retention.[10,12−14,16] At low concentrations of FEC in the electrolyte, the SEI is similar in structure to the SEI generated in the FEC free electrolyte.[10,14]

Received: June 2, 2015
Accepted: August 25, 2015
Published: August 25, 2015

DOI: 10.1021/acsami.5b04845
ACS Appl. Mater. Interfaces 2015, 7, 20004−20011

However, at higher concentrations of FEC, increases in the concentration of LiF and polymeric species are observed in the SEI and cycling performance is improved.[12,13,15,16]

We expand upon our previous investigation of BF silicon nanoparticle electrodes which utilized a combination of XPS, FTIR, TEM, and NMR to characterize the silicon SEI.[15] This investigation utilizes a combination of binder free silicon nanoparticle electrodes (BF-Si) and hard X-ray photoelectron spectroscopy (HAXPES) to develop a better understanding of the role different solvents in SEI structure and composition. Anodes were cycled with $LiPF_6$ in pure ethylene carbonate (EC), pure fluoroethylene carbonate (FEC), and a mixture of EC and FEC. The high photon energies available at synchrotrons (compared with lab sources) significantly increase the probing depth of core level photoemission. As the kinetic energy of the outgoing photoelectrons increases, the mean free path increases as well. Therefore, with the HAXPES technique the elemental composition of thin films such as SEI layers can be probed to greater depths than are available with conventional XPS systems. In addition, the high photon energy can access more tightly bound core electrons such as Si 1s, which are not measurable with traditional XPS.[17] This has enabled additional insight into the depth-dependent structure of the SEI on silicon nanoparticles.

EXPERIMENTAL SECTION

Preparation of Binder-Free Silicon Electrodes and Coin Cell Fabrication. BF-Si electrodes were prepared by electrophoretic deposition (EPD) similar to BF-Si[15] and BF-graphite[19,20] studies previously reported. The EPD bath was prepared by dispersing silicon nanoparticles (~50 nm) in acetonitrile (anhydrous). This method produces electrodes without polymer binders or conductive carbon, being exclusively composed of silicon nanoparticles. The BF-Si electrodes were coated on copper foil with a surface density of ~0.37 mg/cm^2 and vacuum-dried for 24 h at 120 °C. Half cells (CR2032) were fabricated with BF-Si electrodes, a polypropylene separator, and lithium foil in a high purity Ar-filled glovebox with H_2O content <0.1 ppm. Three different electrolytes were used: 1.2 M $LiPF_6$ in EC, 1.2 M $LiPF_6$ in FEC, and 1.2 M $LiPF_6$ in a mix of EC:FEC at a ratio of 85:15 in weight (EC:FEC). Each coin cell contained 30 μL of electrolyte. The cells were cycled 1 or 5 times at 25 °C in the voltage window of 2−0.05 V using a battery cycler at a rate of C/20 for first cycle then C/10 for subsequent cycles. The cycled electrodes were harvested at the discharged state (delithiation) and rinsed four times with DMC (1 mL in total) and dried in glovebox antechamber before ex-situ analysis. The morphology of Si nanoparticles and BF-Si electrode were characterized using a field-emission scanning electron microscopy at 15 kV.

HAXPES Experiments. All HAXPES experiments were conducted at the X-24A end station of the NIST beamline at the National Synchrotron Light Source, Brookhaven National Laboratory (Upton, NY).[21] Synchrotron radiation from a bending magnet is delivered to a constant offset, double Si(111) crystal monochromator via a Ni-coated graphite spherical collimating mirror and vertical and horizontal apertures. Once monochromatized, the beam is focused by a Ni-coated quartz toroidal mirror. The beam spot size is determined just upstream from the analysis chamber by vertical and horizontal apertures. Oriented perpendicular to the beam in the experimental chamber is the entrance aperture of a 200 mm hemispherical analyzer configured to analyze a 0.5 mm spot on the sample positioned in front of it in the analysis chamber. Samples were oriented at grazing incidence to the photon beam, with a takeoff angle toward the analyzer of 3 or 5° relative to the sample normal. This orientation allowed for detection of photoelectrons with the greatest possible mean escape depth. Nominal photon energies and resolutions were determined by measuring the Ag 3d signal from a silver standard foil attached to our sample bar. Total resolution for the analyzer and beamline, established as the half-width of the Fermi edge at the top of the valence band maximum, was measured to be 0.45 and 0.55 eV for excitation energies 2.2 and 4 keV, respectively.

To minimize the samples' exposure to atmosphere, we transferred them to a tightly sealed vessel in an Ar environment for transportation to X-24A and installed them in the experimental chamber through an N_2-filled glovebag. Experimental chamber pressure was less than 6×10^{-7} Pa. The sample bar was electrically connected through the manipulator to a common ground with the analyzer, but no further attempt was made to correct for charging of the samples during measurements.

We observed changes to spectra consistent with photon stimulated desorption of surface species beginning at about 30 min of beam exposure time. To minimize these effects, we collected a minimum number of scans in standardized order at a unique spot on each sample, for each excitation energy, and all necessary spectra for each sample at each photon energy were collected before beam effects were observed. For this investigation photon energies of 2.2 and 4 keV were used. Spectra of Si 1s, F 1s, O 1s, C 1s, and Si 2p electrons were collected at both photon energies. All spectra were recorded with a dwell time of 100 ms and energy step of 0.1 eV, with the analyzer in transmission mode, and all used an analyzer pass energy of 500 eV except the Si 1s electron at 2.2 keV (pass energy 200 eV). The Si 2p spectrum was used for all Si elemental concentrations calculations.

Spectra were analyzed with a commercial software package. All spectra were scaled by the number of scans before subtraction of a Shirley background.[22] Relative atomic concentrations for each element, I_i, were calculated using the following formula: $(I_i = A_i/(T(\mathrm{KE})_i\,\sigma(h\nu)_i\,\lambda(\mathrm{KE})_i))/(\sum_j(A_j/(T(\mathrm{KE})_j\,\sigma(h\nu)_j\,\lambda(\mathrm{KE})_j)))$, where A corresponds to the background-subtracted spectrum area, T is the relative transmission function of the X-24A analyzer,[23] σ is the Scofield photoionization cross-section,[24] λ is the inelastic mean free path of electrons in the material,[25] and the summation index j runs over all distinct elements present in the analysis. Where there were two or more available core electrons per element, we chose the one used in similar calculations for the Al−Kα. Finally, spectra for each core were normalized to the most intense feature for display purposes. XPS experiments were performed with a commercial system using an Al Kα radiation source ($h\nu$ =1486 eV) under ultrahigh vacuum. The displayed binding energy scales for each sample are referenced to a fit of the hydrocarbon peak at 285 eV in the C 1s spectra.

RESULTS

Electrochemical Cycling. Surface morphology of as-prepared Si electrode are presented in Figure 1. The electrode exhibits a smooth surface (Figure 1a) consisting of Si nanoparticles with diameter from 50 to 100 nm (Figure 1b). Voltage profile for the first cycle and capacity retention of BF-Si electrodes in different electrolytes are provided in Figure 2. The cell cycled with 1.2 M $LiPF_6$ in EC has the lowest initial discharge capacity (Figure 2a) and the greatest loss of capacity upon increasing the cycle number from 1 to 5 (Figure 2b). The cells containing EC:FEC have similar first charge and discharge curves and capacity retention to the cells cycled in FEC (Figure 2a). Furthermore, the cells with electrolyte containing FEC outperform the cells with only EC, both in specific capacity and in capacity retention. The excellent cycling performance of Si electrodes with FEC containing electrolytes is likely due to the formation of a good SEI derived from the decomposition of FEC as discussed below.

HAXPES Measurements. The XPS and HAXPES data of silicon electrodes are provided in Figures 3−6 and the elemental concentrations are summarized in Tables 1−3. The plots are arranged in columns corresponding to the depth of penetration and in rows corresponding to the electrolyte formulation (EC top, EC:FEC middle, and FEC bottom). Two spectra are displayed on each plot representing the data from

DOI: 10.1021/acsami.5b04845
ACS Appl. Mater. Interfaces 2015, 7, 20004−20011

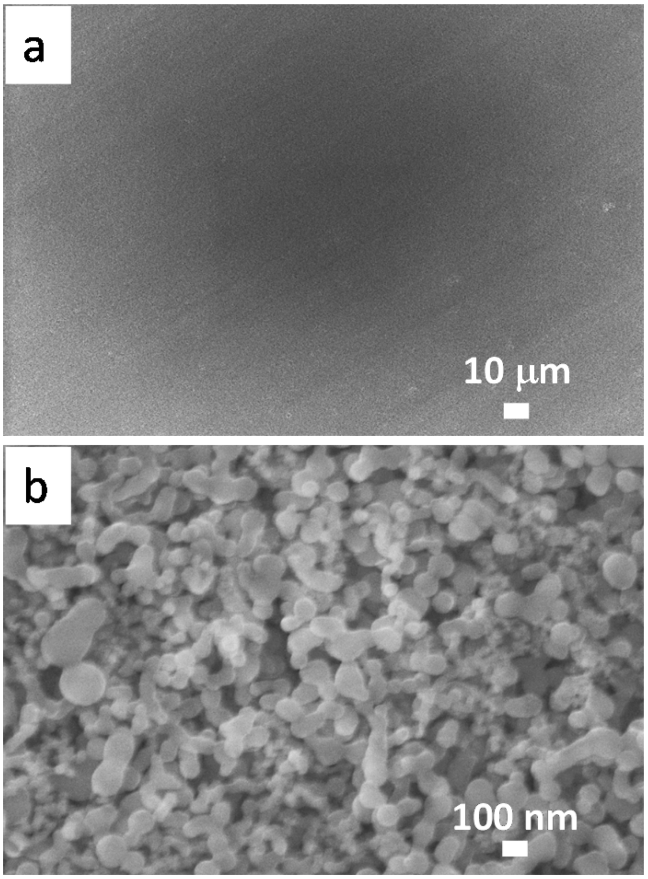

Figure 1. SEM images of a fresh BF-Si at (a) low and (b) high magnification.

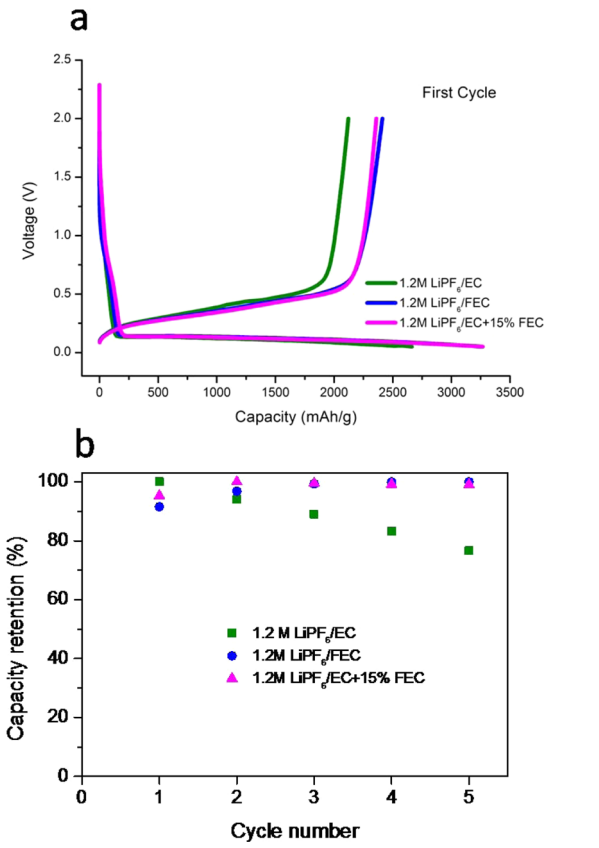

Figure 2. (a) Voltage profile plot for first cycle and (b) capacity retention as a function of cycle number of Si electrodes cycled in different electrolyte.

Table 1. Atomic Concentrations for EC Samples

	Si (%)	F (%)	O (%)	C (%)
		hν = 1487 eV		
fresh	35		46	19
EC-1c	3	2	59	36
EC-5c	4	2	58	36
		hν = 2200 eV		
fresh	42		34	24
EC-1c	10	13	47	30
EC-5c	6	14	46	34
		hν = 4000 eV		
fresh	46		38	16
EC-1c	7	13	53	27
EC-5c	8	17	50	25

the silicon anodes after the first and fifth cycle. The spectra of the fresh electrodes are also provided at the top for elements present in the fresh electrode.

The C 1s spectra are presented in Figure 3. The fresh samples have a peak at 285 eV from hydrocarbon contamination. Upon cycling new peaks are observed in the C 1s XPS spectra of the extracted electrodes and the concentration of C is increased for all electrolytes consistent with the deposition of electrolyte decomposition products on the surface of the silicon anode. The spectra are dominated by new peaks at 286.5 and 290 eV characteristic of C−O- and CO_3-containing species, respectively. The new peaks are characteristic of lithium alkyl carbonates or polycarbonates.[12,13,17,26,27] The XPS spectra also contain a new peak at 288.5 eV characteristic of C═O containing species along with a peak at 285 eV for hydrocarbons.[28] For the electrodes analyzed after one cycle with the EC electrolyte, the spectra are dominated by the new peaks at 286.5 and 290 eV and appear to be similar for all excitation energies (depths of penetration). This suggests that the SEI is primarily composed of lithium ethylene dicarbonate (LEDC)[15,29] and the organic reduction products after the first cycle are consistent throughout the depth of the SEI. However, differences are observed after five cycles. The spectrum obtained at the lowest excitation energy is very similar to the spectrum obtained after one cycle, whereas the spectra obtained at higher excitation energies (deeper depths of penetration) have reduced intensity for the peak at 290 eV and an increase in the intensity of the peak at 288.5 eV. However, the concentration of C does not change significantly with increased cycling. The similarity of the intensity of the CO_3 peak at the surface and decreases in intensity of the $-CO_3$ peak in the interior is consistent with fresh electrolyte reduction to generate LEDC in the outer SEI and LEDC decomposition in the inner SEI. Previous reports suggest that LEDC is unstable and can decompose to generate carbon dioxide (CO_2), lithium oxalate, Li_2CO_3, and lithium alkoxides.[27,30−32]

The XPS spectra of the electrode cycled with EC:FEC electrolyte after one cycle are very similar to those with EC electrolyte. The spectra at all three excitation energies are again similar suggesting a comparable composition of organic decomposition products throughout the SEI. However, after five cycles the XPS spectra have very little change, suggesting

DOI: 10.1021/acsami.5b04845
ACS Appl. Mater. Interfaces 2015, 7, 20004−20011

Table 2. Atomic Concentrations for EC:FEC Samples

	Si (%)	F (%)	O (%)	C (%)
		$h\nu$ = 1487 eV		
fresh	35		46	19
EC:FEC-1c	2	7	52	39
EC:FEC-5c	6	13	45	36
		$h\nu$ = 2200 eV		
fresh	52		28	20
EC:FEC-1c	3	3	54	40
EC:FEC-5c	2	8	45	45
		$h\nu$ = 4000 eV		
fresh	55		30	15
EC:FEC-1c	5	3	57	35
EC:FEC-5c	4	9	50	37

Table 3. Atomic Concentrations for FEC Samples

	Si (%)	F (%)	O (%)	C (%)
		$h\nu$ = 1487 eV		
fresh	35		46	19
FEC-1c	4	7	38	51
FEC-5c	4	14	25	57
		$h\nu$ = 2200 eV		
fresh	42		34	24
FEC-1c	5	22	37	36
FEC-5c	4	20	40	36
		$h\nu$ = 4000 eV		
fresh	46		38	16
FEC-1c	5	26	38	32
FEC-5c	4	22	43	31

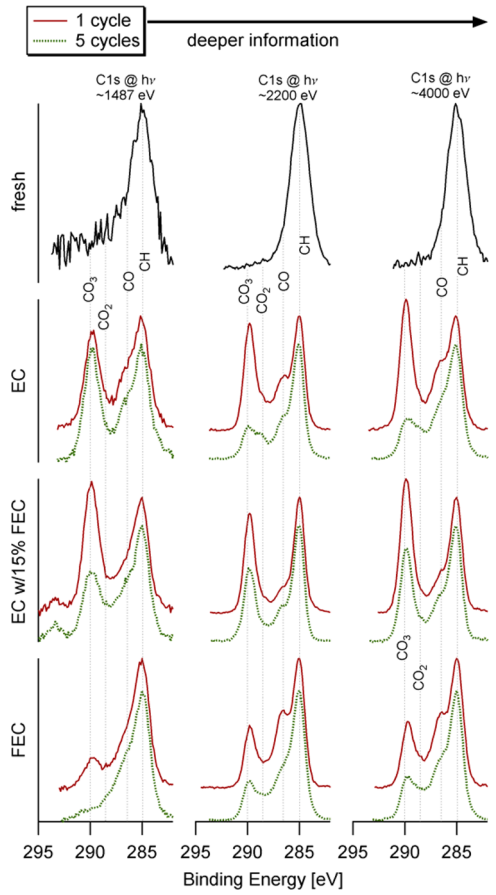

Figure 3. Carbon 1s spectra of pristine BF-Si anodes (top row) and for first (red) and fifth (green) cycle BF-Si anodes from coin cells fabricated with electrolyte solvent EC (2nd row), EC:FEC (3rd row), and FEC (bottom row).

that the presence of the FEC reduction products inhibit the decomposition of the SEI components.

The XPS spectra of the electrode cycled with the FEC electrolyte after the first cycle are similar to the XPS spectra of the electrodes cycled with the EC or EC:FEC electrolytes, except that the intensity of the peak at 290 eV, associated with CO_3-containing species is significantly weaker. This is likely due to the presence of poly(FEC) and absence of LEDC on the silicon surface.[12,15] The spectra are also largely independent of the excitation energy suggesting the organic components are similar in the inner and outer SEI. Upon increasing the number of cycles from 1 to 5, the carbon spectra do not markedly change, suggesting the C containing components of the SEI generated from the FEC electrolyte are more stable than the C-containing components of the SEI generated from the EC electrolyte.

The XPS and HAXPES silicon spectra including both the 1s and 2p core levels are provided in Figure 4. The binding energy of Si 1s is ~1,840 eV which is approximately 20 times higher than binding energy of the Si 2p (~99 eV). Thus, the Si 1s electron has less kinetic energy than Si 2p at the same excitation energy. As a result, the peak observed from the 1s electron originates from a shallower average depth in the sample than the peak observed for the 2p electron. The far left column displays 1s spectra acquired with 2,200 eV photons, which provides a more surface sensitive measurement than the standard XPS spectrum for the Si 2p signal displayed in the middle left column. The far right column represents information for the Si 2p electron at 4,000 eV and is the most bulk-sensitive measurement for silicon. The top row depicts the Si spectra for the fresh silicon anodes and demonstrates the capability of depth profiling. The Si spectrum for the most surface sensitive measurement (Si 1s @ 2200 eV) contains a large peak characteristic of SiO_2 at 1843 eV and a small peak characteristic of Si−Si at 1839 eV[33] consistent with a native oxide layer encapsulating the Si nanoparticles. As the depth of penetration is steadily increased from the far left column to the far right column, the intensity ratio of the SiO_2 to Si−Si peaks gradually change until the Si−Si peak is dominant and the SiO_2 peak is small. This is consistent with a gradual increase in the depth of penetration and the thin SiO_2 layer having a smaller influence on the overall spectrum.

Upon analysis of the cycled anodes, the peaks attributed to elemental silicon (1s: 1839 eV and Si 2p: 99 eV)[17,33] are not present for any of the electrolytes. The exterior surface of the silicon anodes (least penetration, far left column) cycled with the EC electrolyte are dominated by SiO_2 with low concentrations of Li_xSiO_y (100.5, Si 2p; 1840, Si 1s).[17,34] As the depth of penetration is increased the relative intensity of the SiO_2 peaks is decreased and the Li_xSiO_y peaks are increased. In addition, at the greatest depth of penetration Li_xSi (1837 eV, Si 1s; 97 eV, Si 2p)[17,34] becomes observable in low concentrations. The maximum mean free path for these photoelectrons suggests that the SEI is approximately 10 nm thick. The silicon spectra of the electrodes analyzed after five cycles with the EC electrolyte are very similar to the silicon spectra after the first cycle.

DOI: 10.1021/acsami.5b04845
ACS Appl. Mater. Interfaces 2015, 7, 20004−20011

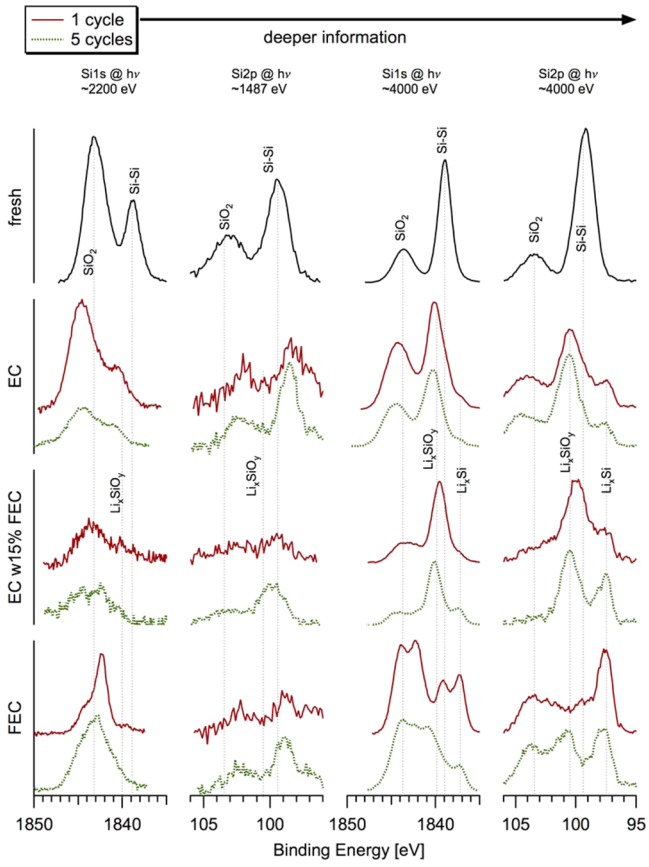

Figure 4. Silicon spectra of pristine BF-Si anodes (top row) and for first (red) and fifth (green) cycle anodes from coin cells fabricated with electrolyte solvent EC (2nd row), EC:FEC (3rd row), and FEC (bottom row).

The silicon spectra of the electrodes cycled with the EC:FEC electrolyte have similar peaks to the electrodes cycled with the EC electrolyte. In addition, only small changes are observed upon increasing the number of cycles from 1 to 5. However, the appearance of the peak associated with Li_xSi is observed at shallower depths of penetration, which suggests that the SEI may be thinner with added FEC.

The silicon spectra of the electrode cycled with the FEC electrolyte after one cycle have differences compared to the electrodes cycled with electrolyte containing EC. The exterior surface of the silicon (far left column) is dominated by peaks associated with SiO_2, but the Li_xSiO_y peaks are absent. As the depth of penetration is increased this trend continues. The peaks of the Li_xSiO_y which dominate the spectra for the middle two columns of spectra after one cycle for the EC and EC:FEC electrolytes are not present. Although the spectra are complicated by differential charging effects that result in a doubling of some of the peaks, the only two peaks observed are associated with SiO_2 and Li_xSi.[28,35] As expected, the peak associated with the Li_xSi becomes dominant at the greatest depth of penetration. After 5 cycles differences are observed for the FEC electrolyte, especially at the greater depths of penetration. Peaks associated with Li_xSiO_y, absent after the first cycle, become apparent, suggesting that the silicon containing species evolve with continued cycling, whereas the carbon containing species, as described above, remain constant with additional cycling. Interestingly, the concentration of Si does not significantly increase as a function of depth of penetration for all electrolytes investigated as one would expect. This may relate to limitations related to the quantification of XPS.

The XPS and HAXPES F 1s spectra are provided in Figure 5 and the elemental concentrations are summarized in Tables

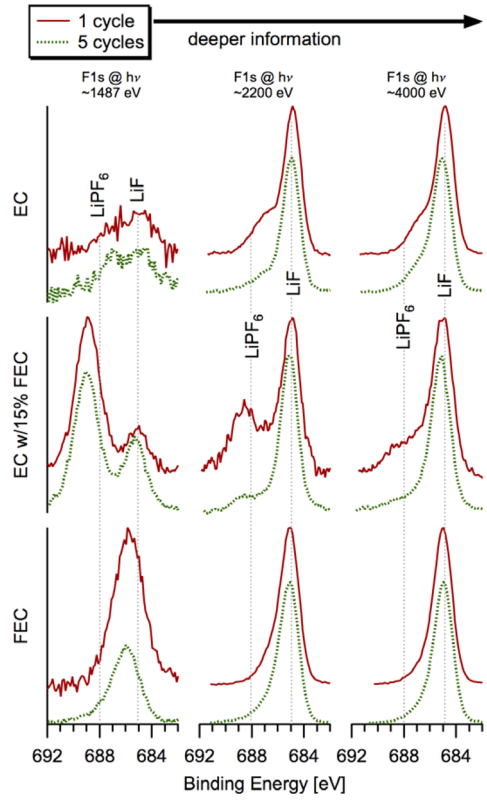

Figure 5. Fluorine 1s spectra for the first (red) and fifth (green) cycle BF-Si anodes from coin cells fabricated with electrolyte solvent EC (1st row), EC:FEC (2nd row), and FEC (3rd row).

1−3. All spectra exhibit a peak at 685 eV, attributed to LiF, as well as a shoulder or peak at higher binding energy which indicates the presence of residual $LiPF_6$ salt or $Li_xPF_yO_z$.[10,12−18,36] The peaks associated with $LiPF_6$ are strongest for the spectra with the lowest depth of penetration consistent with incomplete removal of the $LiPF_6$ from the electrode surface during washing. The relative atomic concentrations for the electrodes cycled with the EC electrolyte as a function of depth of penetration (Table 1) reveal that the concentration of F is lowest in the outer SEI and greater in the inner SEI, but that the F concentration does not change significantly with increased cycles. A different trend is observed for the EC:FEC electrolyte (Table 2). The concentration of F is greatest at the surface (shallowest depth of penetration) and decreases with increased depth of penetration. However, the higher concentration of F may be related to the higher concentration of residual $LiPF_6$. In addition, the concentration of F increases with increased cycling. The trend for the FEC electrolyte is similar to that observed for the EC electrolyte except that the concentration of F is higher. The concentration of F in the outer SEI is lower than in the inner SEI and changes to the F concentration with increased cycles are small.

Oxygen concentrations are reported in Tables 1−3, and the spectra are displayed in Figure 6. The O 1s spectrum of the fresh electrode contains a broad peak at 532 eV characteristic of

DOI: 10.1021/acsami.5b04845
ACS Appl. Mater. Interfaces 2015, 7, 20004−20011

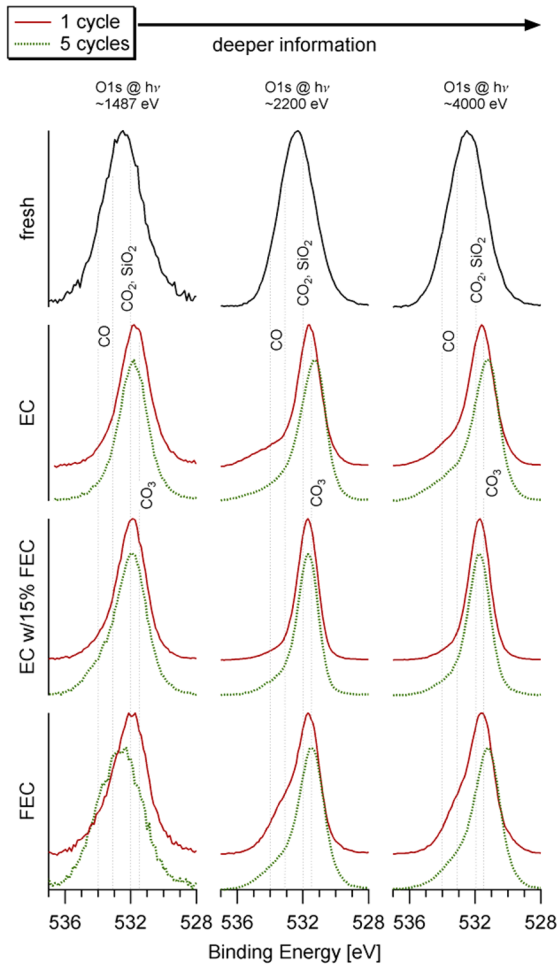

Figure 6. Oxygen 1s spectra of pristine BF-Si anodes (top row) and for first (red) and fifth (green) cycle BF-Si anodes from coin cells fabricated with electrolyte solvent EC (2nd row), EC:FEC (3rd row), and FEC (bottom row).

SiO_2.[17] The oxygen concentration is highest for the shallowest depth of penetration consistent with SiO_2 on the surface of the particle. Upon cycling the O 1s peak is shifted to ~531.5 eV for all electrolytes investigated and remains broad, consistent with the presence of C−O, C═O, and Si−O bonds.[12,17,18] The concentration of O is increased for all electrolytes although the increases are smallest for the FEC electrolyte. There is an additional high energy shoulder for electrodes cycled with FEC at 534 eV consistent with the presence of poly(FEC).[12] However, the changes in the O concentrations as a function of depth of penetration or additional cycling are small.

DISCUSSION

The SEI generated on BF-Si nanoparticle anodes cycled with 1.2 M $LiPF_6$ in EC, FEC, and EC:FEC electrolytes were investigated by electrochemical cycling and HAXPES. Electrochemical cycling data show only small differences between the performance of the FEC and EC:FEC electrolytes. However, cells cycled with electrolyte containing FEC cycle better than the electrolyte containing only EC. This suggests the FEC additive has a significant influence on the SEI generated on the silicon nanoparticle anodes. A schematic representation of the surface films is provided in Figure 7. Although the data are consistent with Li_xSiO_y and SiO_2 at the same depth of

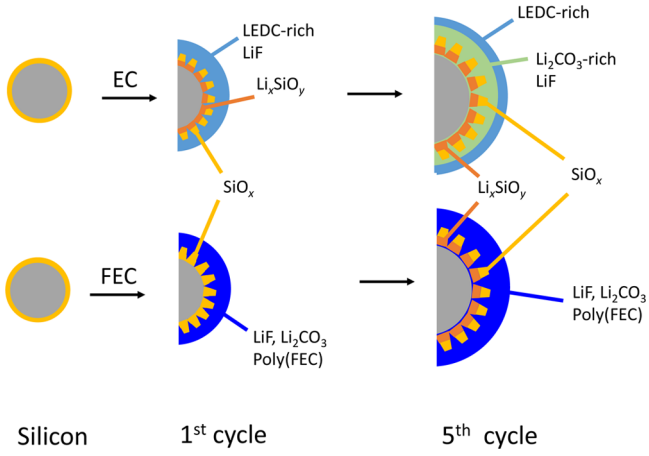

Figure 7. Schematic depiction of SEI on silicon nanoparticles with different electrolytes.

penetration as the electrolyte decomposition products, the nature of the intermixing of the materials is unclear.

The HAXPES investigation of the silicon nanoparticles cycled with different electrolytes reveals that the changes in the electrolyte composition result in changes to surface film structures upon cycling. In all cases, the SEI generated on the surface is composed of electrolyte decomposition products which are integrated with silicon containing species. Otherwise each of the different electrolytes has different surface film components.

For $LiPF_6$ in EC electrolyte, the surface film is primarily composed of LEDC and LiF from the reduction of EC and $LiPF_6$, respectively, along with lower concentrations of Li_2CO_3.and lithium alkoxides. After the first cycle the LEDC dominates the outer SEI whereas the concentration of LiF increases in the inner SEI. Upon cycling the concentrations of C, O, and F do not change significantly, but the LEDC decomposes into carbon dioxide, lithium oxalate, Li_2CO_3, and lithium alkoxides.[30] This suggests that the LEDC is unstable in the SEI on silicon upon continuous cycling. This decomposition reaction likely contributes to cell inefficiency and capacity loss. The silicon-containing species intermixed with the SEI are dominated by SiO_2 in the outer SEI and Li_xSiO_y in the inner SEI. The composition of the silicon component does not change significantly upon increased cycling.

The surface film generated with the EC:FEC electrolyte is also dominated by LEDC but also contains LiF and poly(FEC). The results are consistent with those previously reported.[37] In contrast to the observation with EC, the LiF concentration is higher in the outer SEI and lower in the inner SEI. With additional cycling, the concentration of F increases, but interestingly the LEDC does not decompose in the inner SEI. This suggests that the presence of the FEC reduction products, poly(FEC) and additional LiF, inhibit LEDC decomposition upon additional cycling. The silicon-containing species incorporated into the SEI are very similar to that observed for $LiPF_6$ in EC. SiO_2 is the dominant species intermixed with the outer SEI and Li_xSiO_y is the dominant species intermixed with the inner SEI. However, the SEI for the EC:FEC electrolyte is slightly thinner than the SEI with the EC electrolyte because the concentration of the Li_xSi at the deepest depth of penetration is slightly greater for the electrode cycled with the EC:FEC electrolyte than it is for the electrode cycled with the EC electrolyte.

DOI: 10.1021/acsami.5b04845
ACS Appl. Mater. Interfaces 2015, 7, 20004−20011

A very different ratio of CO_3 to C−O is observed with the $LiPF_6$ in FEC electrolyte, consistent with the generation of poly(FEC). The composition of organic species is relatively consistent through the depth of the SEI and the changes upon cycling are quite small. The silicon containing species are different than what are observed for the EC containing electrolytes. While SiO_2 is observed intermixed with the outer SEI there is no Li_xSiO_y intermixed with the inner SEI only Li_xSi. The results are unusual because previous reports have suggested that Li_xSiO_y is generated from the residual SiO_2 on the silicon surface during lithiation.[37] This suggests that either the FEC reduction products, poly(FEC) and LiF, inhibit the generation of Li_xSiO_y or that the Li_xSiO_y may be generated from the lithium alkyl carbonates. Upon additional cycling, the changes to the organic components are small, but changes to the silicon containing species are observed. Li_xSiO_y is observed which suggests that either the initial inhibition of Li_xSiO_y generation from SiO_2 is discontinued or the secondary decomposition products of poly(FEC) could lead to Li_xSiO_y. At this time, we do not have a good understanding of this unusual trend in Li_xSiO_y appearance.

CONCLUSIONS

Binder-free silicon (BF-Si) nanoparticle anodes have been cycled with three different electrolytes: 1.2 M $LiPF_6$ in ethylene carbonate (EC), fluoroethylene carbonate (FEC), or EC:FEC. Electrolytes containing FEC had the best capacity retention after five cycles. The electrodes were extracted and analyzed by hard X-ray photoelectron spectroscopy (HAXPES) to determine changes to the SEI upon changes in electrolyte. All of the electrolytes generate an SEI, which is integrated with Si-containing species and contain the decomposition products of the electrolyte. The electrolytes with the best performance (FEC and EC:FEC) have electrolyte decomposition products in the SEI that are stable upon additional cycling. The electrolyte with the poorest capacity retention (EC) has the greatest changes to the composition of the SEI upon cycling, consistent with poor SEI component stability upon cycling.

AUTHOR INFORMATION

Corresponding Author

*E-mail: blucht@chm.uri.edu.

Notes

The authors declare no competing financial interest.

ACKNOWLEDGMENTS

We gratefully acknowledge funding from Department of Energy, Office of Basic Energy Sciences, EPSCoR Implementation award (DE-SC0007074). Use of the National Synchrotron Light Source, Brookhaven National Laboratory, was supported by the U.S. Department of Energy, Office of Science, Office of Basic Energy Sciences, under Contract DE-AC02-98CH10886. Additional support was provided by the National Institute of Standards and Technology (J.C.W.).

REFERENCES

(1) Obrovac, M. N.; Christensen, L. Structural Changes in Silicon Anodes during Lithium Insertion/Extraction. *Electrochem. Solid-State Lett.* **2004**, *7*, A93−A96.

(2) Benedek, R.; Thackeray, M. M. Lithium Reactions with Intermetallic-Compound Electrodes. *J. Power Sources* **2002**, *110*, 406−411.

(3) Chon, M. J.; Sethuraman, V. A.; McCormick, A.; Srinivasan, V.; Guduru, P. R. Real-Time Measurement of Stress and Damage Evolution during Initial Lithiation of Crystalline Silicon. *Phys. Rev. Lett.* **2011**, *107*, 045503.

(4) Wu, H.; Cui, Y. Designing Nanostructured Si Anodes for High Energy Lithium Ion Batteries. *Nano Today* **2012**, *7*, 414−429.

(5) Ng, S.-H.; Wang, J.; Wexler, D.; Konstantinov, K.; Guo, Z.-P.; Liu, H.-K. Highly Reversible Lithium Storage in Spheroidal Carbon-Coated Silicon Nanocomposites as Anodes for Lithium-Ion Batteries. *Angew. Chem., Int. Ed.* **2006**, *45*, 6896−6899.

(6) Kim, H.; Han, B.; Choo, J.; Cho, J. Three-Dimensional Porous Silicon Particles for Use in High-Performance Lithium Secondary Batteries. *Angew. Chem., Int. Ed.* **2008**, *47*, 10151−10154.

(7) Magasinski, A.; Dixon, P.; Hertzberg, B.; Kvit, A.; Ayala, J.; Yushin, G. High-Performance Lithium-Ion Anodes Using a Hierarchical Bottom-up Approach. *Nat. Mater.* **2010**, *9*, 353−358.

(8) Chevrier, V. L.; Liu, L.; Le, D. B.; Lund, J.; Molla, B.; Reimer, K.; Krause, L. J.; Jensen, L. D.; Figgemeier, E.; Eberman, K. W. Evaluating Si-Based Materials for Li-Ion Batteries in Commercially Relevant Negative Electrodes. *J. Electrochem. Soc.* **2014**, *161*, A783−A791.

(9) Chen, L.; Wang, K.; Xie, X.; Xie, J. Enhancing Electrochemical Performance of Silicon Film Anode by Vinylene Carbonate Electrolyte Additive. *Electrochem. Solid-State Lett.* **2006**, *9*, A512−A512.

(10) Choi, N.-S.; Yew, K. H.; Lee, K. Y.; Sung, M.; Kim, H.; Kim, S.-S. Effect of Fluoroethylene Carbonate Additive on Interfacial Properties of Silicon Thin-Film Electrode. *J. Power Sources* **2006**, *161*, 1254−1259.

(11) Song, S.-W.; Baek, S.-W. Silane-Derived SEI Stabilization on Thin-Film Electrodes of Nanocrystalline Si for Lithium Batteries. *Electrochem. Solid-State Lett.* **2009**, *12*, A23−A27.

(12) Etacheri, V.; Haik, O.; Goffer, Y.; Roberts, G. a; Stefan, I. C.; Fasching, R.; Aurbach, D. Effect of Fluoroethylene Carbonate (FEC) on the Performance and Surface Chemistry of Si-Nanowire Li-Ion Battery Anodes. *Langmuir* **2012**, *28*, 965−976.

(13) Nakai, H.; Kubota, T.; Kita, A.; Kawashima, A. Investigation of the Solid Electrolyte Interphase Formed by Fluoroethylene Carbonate on Si Electrodes. *J. Electrochem. Soc.* **2011**, *158*, A798−A798.

(14) Dalavi, S.; Guduru, P.; Lucht, B. L. Performance Enhancing Electrolyte Additives for Lithium Ion Batteries with Silicon Anodes. *J. Electrochem. Soc.* **2012**, *159*, A642−A646.

(15) Nie, M.; Abraham, D. P.; Seo, D. M.; Chen, Y.; Bose, A.; Lucht, B. L.; Chalasani, D. Silicon Solid Electrolyte Interphase (SEI) of Lithium Ion Battery Characterized by Microscopy and Spectroscopy. *J. Phys. Chem. C* **2013**, *117*, 13403−13412.

(16) Nguyen, C. C.; Lucht, B. L. Comparative Study of Fluoroethylene Carbonate and Vinylene Carbonate for Silicon Anodes in Lithium Ion Batteries. *J. Electrochem. Soc.* **2014**, *161*, A1933−A1938.

(17) Philippe, B.; Dedryvère, R.; Allouche, J.; Lindgren, F.; Gorgoi, M.; Rensmo, H.; Gonbeau, D.; Edström, K. Nanosilicon Electrodes for Lithium-Ion Batteries: Interfacial Mechanisms Studied by Hard and Soft X-Ray Photoelectron Spectroscopy. *Chem. Mater.* **2012**, *24*, 1107−1115.

(18) Philippe, B.; Dedryvère, R.; Gorgoi, M.; Rensmo, H.; Gonbeau, D.; Edström, K.; Edstro, K. Role of the LiPF 6 Salt for the Long-Term Stability of Silicon Electrodes in Li-Ion Batteries − A Photoelectron Spectroscopy Study. *Chem. Mater.* **2013**, *25*, 394−404.

(19) Kang, S.-H.; Abraham, D. P.; Xiao, A.; Lucht, B. L. Investigating the Solid Electrolyte Interphase Using Binder-Free Graphite Electrodes. *J. Power Sources* **2008**, *175*, 526−532.

(20) Xiao, A.; Yang, L.; Lucht, B. L.; Kang, S.-H.; Abraham, D. P. Examining the Solid Electrolyte Interphase on Binder-Free Graphite Electrodes. *J. Electrochem. Soc.* **2009**, *156*, A318−A327.

(21) Weiland, C.; Rumaiz, A. K.; Lysaght, P.; Karlin, B.; Woicik, J. C.; Fischer, D. NIST High Throughput Variable Kinetic Energy Hard X-Ray Photoelectron Spectroscopy Facility. *J. Electron Spectrosc. Relat. Phenom.* **2013**, *190*, 193−200.

(22) Shirley, D. A. High-Resolution X-Ray Photoemission Spectrum of the Valence Bands of Gold. *Phys. Rev. B* **1972**, *5*, 4709−4714.

DOI: 10.1021/acsami.5b04845
ACS Appl. Mater. Interfaces 2015, 7, 20004−20011

(23) Weiland, C.; Browning, R.; Karlin, B. A.; Fischer, D. A.; Woicik, J. C. Note: Alignment/focus Dependent Core-Line Sensitivity for Quantitative Chemical Analysis in Hard X-Ray Photoelectron Spectroscopy Using a Hemispherical Electron Analyzer. *Rev. Sci. Instrum.* **2013**, *84*, 036106.
(24) Scofield, J. H. *Theoretical Photoionization Cross Sections from 1 to 1500 keV.*; UCRL−51326, 4545040 ; Lawrence Livermore Laboratory: Livermore, CA, 1973.
(25) Painter, L. R.; Arakawa, E. T.; Williams, M. W.; Ashley, J. C. Optical Properties of Polyethylene: Measurement and Applications. *Radiat. Res.* **1980**, *83*, 1−18.
(26) Gireaud, L.; Grugeon, S.; Laruelle, S.; Pilard, S.; Tarascon, J.-M. Identification of Li Battery Electrolyte Degradation Products Through Direct Synthesis and Characterization of Alkyl Carbonate Salts. *J. Electrochem. Soc.* **2005**, *152*, A850−A857.
(27) Xu, K.; Zhuang, G. V.; Allen, J. L.; Lee, U.; Zhang, S. S.; Ross, P. N.; Jow, T. R. Syntheses and Characterization of Lithium Alkyl Mono- and Dicarbonates as Components of Surface Films in Li-Ion Batteries. *J. Phys. Chem. B* **2006**, *110*, 7708−7719.
(28) Moulder, J. F.; Chastain, J. *Handbook of X-Ray Photoelectron Spectroscopy: A Reference Book of Standard Spectra for Identification and Interpretation of XPS Data*; Physical Electronics Division, Perkin-Elmer Corp.: Eden Prairie, MN, 1992.
(29) Zhuang, G. V.; Xu, K.; Yang, H.; Jow, T. R.; Ross, P. N.; Ross, P. N., Jr. Lithium Ethylene Dicarbonate Identified as the Primary Product of Chemical and Electrochemical Reduction of EC in 1.2 M LiPF6/EC:EMC Electrolyte. *J. Phys. Chem. B* **2005**, *109*, 17567−17573.
(30) Seo, D. M.; Chalasani, D.; Parimalam, B. S.; Kadam, R.; Nie, M.; Lucht, B. L. Reduction Reactions of Carbonate Solvents for Lithium Ion Batteries. *ECS Electrochem. Lett.* **2014**, *3*, A91−A93.
(31) Zhuang, G. V.; Yang, H.; Ross, P. N.; Xu, K.; Jow, T. R. Lithium Methyl Carbonate as a Reaction Product of Metallic Lithium and Dimethyl Carbonate. *Electrochem. Solid-State Lett.* **2006**, *9*, A64−A68.
(32) Zhuang, G. V.; Ross, P. N. Analysis of the Chemical Composition of the Passive Film on Li-Ion Battery Anodes Using Attentuated Total Reflection Infrared Spectroscopy. *Electrochem. Solid-State Lett.* **2003**, *6*, A136−A139.
(33) Yabuuchi, N.; Shimomura, K.; Shimbe, Y.; Ozeki, T.; Son, J.-Y.; Oji, H.; Katayama, Y.; Miura, T.; Komaba, S. Graphite-Silicon-Polyacrylate Negative Electrodes in Ionic Liquid Electrolyte for Safer Rechargeable Li-Ion Batteries. *Adv. Energy Mater.* **2011**, *1*, 759−765.
(34) Philippe, B.; Dedryvère, R.; Gorgoi, M.; Rensmo, H.; Gonbeau, D.; Edström, K. Improved Performances of Nanosilicon Electrodes Using the Salt LiFSI: A Photoelectron Spectroscopy Study. *J. Am. Chem. Soc.* **2013**, *135*, 9829−9842.
(35) Yu, X.; Hantsche, H. Some Aspects of the Charging Effect in Monochromatized Focused XPS. *Fresenius' J. Anal. Chem.* **1993**, *346*, 233−236.
(36) Edström, K.; Herstedt, M.; Abraham, D. P. A New Look at the Solid Electrolyte Interphase on Graphite Anodes in Li-Ion Batteries. *J. Power Sources* **2006**, *153*, 380−384.
(37) Xu, C.; Lindgren, F.; Philippe, B.; Gorgoi, M.; Björefors, F.; Edström, K.; Gustafsson, T. Improved Performance of the Silicon Anode for Li-Ion Batteries: Understanding the Surface Modification Mechanism of Fluoroethylene Carbonate as an Effective Electrolyte Additive. *Chem. Mater.* **2015**, *27*, 2591−2599.

DOI: 10.1021/acsami.5b04845
ACS Appl. Mater. Interfaces 2015, 7, 20004−20011